Journal of Non-Crystalline Solids 355 (2009) 2148–2155

Contents lists available at ScienceDirect

Journal of Non-Crystalline Solids

journal homepage: www.elsevier.com/locate/jnoncrysol

X-ray photoelectron spectroscopy (XPS) and magnetic susceptibility studies of vanadium phosphate glasses

G.D. Khattak [a], A. Mekki [a], L.E. Wenger [b,*]

[a] Department of Physics, King Fahd University of Petroleum and Minerals, Dhahran 31261, Saudi Arabia
[b] Department of Physics, The University of Alabama at Birmingham, Birmingham, AL 35294-1170, USA

ARTICLE INFO

Article history:
Received 23 May 2008
Received in revised form 16 June 2009
Available online 6 August 2009

PACS:
61.05.js
61.43.Fs
75.20.-g

Keywords:
Magnetic properties
Oxide glasses
Phosphates
XPS

ABSTRACT

Vanadium phosphate glasses with the nominal chemical composition $[(V_2O_5)_x(P_2O_5)_{1-x}]$, where $x = 0.30$, 0.40, 0.50, and 0.60, have been prepared and investigated by X-ray photoelectron spectroscopy (XPS) and magnetization measurements. Asymmetries found in the O 1s, P 2p, and V 2p core level spectra indicate the presence of primarily P–O–P, P–O–V, and V–O–V structural bonds, a spin–orbit splitting of the P 2p core level, and more than one valence state of V ions being present. The magnetic susceptibility data for these glasses follow a Curie–Weiss behavior which also indicates the presence of some V ions existing in a magnetic state, i.e., a valence state other than that of the non-magnetic V^{5+}. From qualitative comparisons of the abundance of the bridging oxygen or P–O–P sites as determined from the areas under the various O 1s peaks with the abundances of differing phosphate structural groups associated with the presence of different valence states of the vanadium ions, a glass structure model consisting of a mixture of vanadate phosphate phases is proposed for these glass samples. These include V_2O_5, $VOPO_4$, $(VO)_2P_2O_7$, $VO(PO_3)$, and $V(PO_3)_3$ with the abundance of orthophosphate $(PO_4)^{3-}$ units increasing with increasing vanadium content.

1. Introduction

Vanadate and phosphate glasses continue to be of interest because of their unique properties and correspondingly their potential suitability for applications. For example, binary and ternary V_2O_5 glasses can exhibit a semiconducting behavior [1–4] which arises from an unpaired $3d^1$ electron hopping between the transition metal (TM) ions [5–6] when the TM ions exist in two or more valence states, i.e., an electron hopping from a V^{4+} site to a V^{5+} site. On the other hand, the low thermo-optical coefficient and large emission characteristics found in phosphate glasses make them suitable materials for high power laser devices [7]. Furthermore, most biocompatible glasses are based on phosphate glasses. In either glass system, however, information on the structure of a glass is imperative for understanding the glass properties and assessing their suitability for applications.

The basic structure of vitreous phosphate consists of PO_4 tetrahedra connected on the three of the four corners with the fourth corner being occupied by terminal double-bonded oxygen [8]. The introduction of a glass modifier such as RO or R_2O with O/P ratios of less than 3 results in a breaking of the covalent P–O–P bonds with additional terminal oxygen P=O bonds or P–O–R bonds being formed. Depending on the number of remaining bridging oxygen, the phosphate tetrahedra can be classified using the Q^i terminology [8–12], where '*i*' represents the number of bridging oxygen sites per tetrahedron. Thus Q^3 refers to a fully polymerized structure, while Q^2 denotes a two-dimensional structure based on chains or rings which is characteristic of a metaphosphate structure with 2 bridging oxygen and 2 non-bridging oxygen. A PO_4 tetrahedron connected by a corner to another PO_4 tetrahedron as in the pyrophosphate P_2O_7 structure is denoted by Q^1 with 1 bridging oxygen while the isolated tetrahedron with no bridging oxygen as in the orthophosphate PO_4 structure are represented by Q^0.

In comparison, the structure of vanadate glasses is less clear as to the exact nature of the oxygen polyhedra surrounding the vanadium atoms or of the role played by the other glass components. For example, structural studies on alkaline earth vanadate glasses by NMR and IR spectroscopy techniques [13–15] suggest that the local structure of these glasses is basically the same irrespective of the alkaline earth metal and consists mainly of corner-sharing VO_4-tetrahedra. Yet, neutron diffraction investigations on other vanadate glasses [16–17] indicate that the vanadate network is composed of distorted, interconnected VO_5 trigonal bipyramids/tetragonal pyramids with the modifier metal ions being randomly dispersed in holes of the vanadate network. Moreover other

* Corresponding author. Address: Department of Physics, The University of Alabama at Birmingham, Birmingham, CH 464, 1530 3rd Avenue S, AL 35294-1170, USA. Tel.: +1 205 934 5102; fax: +1 205 975 6111.
E-mail address: wenger@uab.edu (L.E. Wenger).

0022-3093/$ - see front matter © 2009 Elsevier B.V. All rights reserved.
doi:10.1016/j.jnoncrysol.2009.06.042

structural studies have reported that V_2O_5 acts as a network former [18–19] and consists of unaffected VO_5 groups as in vitreous V_2O_5 and affected VO_5 groups with alkaline earth ions. This is in contrast to studies suggesting that the vanadate glasses behave as a conventional network former in which only unaffected VO_5 groups are present [20]. Even in the case of pure V_2O_5 glass it has been reported [21–22] that V^{5+} ions exhibit both fourfold and fivefold coordination states depending upon the sample preparation conditions. Thus the structure of the vanadate glasses may not only be dependent on the network modifier but also on the nature of vanadate network itself.

Structural studies on the vanadate phosphate glass system are even more limited. Early NMR data [23] on a series of vanadate-rich phosphate glasses were interpreted in terms of two types of VO_5 units being present in this glass system, one being similar to that in crystalline V_2O_5 and the other having a VO_5 unit with a PO_4 unit substituted for the apex oxygen. In addition, both NMR and ESR (electron spin resonance) data indicated the presence of both V^{5+} and V^{4+} ions with two V^{4+} sites being formed for each PO_4 unit substituted at the apex oxygen of the VO_5 unit. Another ESR study [24] reported that V^{5+} and V^{4+} ions co-existed for high vanadium oxide content glasses while either lower vanadium oxidation states were produced in smaller concentrated V_2O_5 glasses or V^{4+} ions existed at sites different from those giving rise to a ESR signal. A neutron diffraction study [17] on vanadate-rich P_2O_5–V_2O_5 glasses (O/P > 5) concluded that the glass structure was composed of a vanadate chain-like network consisting of distorted VO_5 tetragonal pyramids with these chains cross-linked by PO_4 tetrahedra and having all four P–O bond lengths the same.

Since X-ray photoelectron spectroscopy (XPS) has proven to be an important technique in the study of the local structure of oxide glasses, an XPS study on a series of moderately concentrated V_2O_5–P_2O_5 glasses (3.5 < O/P < 6) should be beneficial in further elucidating the nature of glass structure in this system. Distinguishing different types of oxygen sites, e.g., bridging oxygen (BO) versus non-bridging oxygen (NBO) [25–29], as a function of vanadate concentration can be especially important in understanding whether the role of vanadate changes from being a network modifier to a network former. In addition, the valence state of the TM ions in the glass structure can be investigated and their relative concentrations can be determined [30]. Moreover, magnetization measurements combined with inductively coupled plasma (ICP) spectroscopy can provide an independent determination of the ratio of the different valence states of V present in these glasses.

2. Experimental details

2.1. Glass preparation

All glasses were prepared by melting dry mixtures of reagent grade V_2O_5 and P_2O_5 in alumina crucibles to form nominal $[(V_2O_5)_x(P_2O_5)_{1-x}]$ compositions with $x = 0.30$, 0.40, 0.50 and 0.60. Since oxidation and reduction reactions in a glass melt are known to depend on the size of the melt, on the sample geometry, on whether the melt is static or stirred, on thermal history, and on quenching rate, all glass samples were prepared under similar conditions to minimize these factors. Approximately 20 g of chemicals were thoroughly mixed to obtain a homogenized mixture for each V_2O_5 concentration. The crucible containing the batch mixture was then placed in an electrically heated melting furnace and maintained at 1000–1100 °C for about 1-to-2 h under atmospheric conditions during which the melt was occasionally stirred with an alumina rod. The homogenized melt was then cast onto a stainless steel plate mold to form glass buttons and glass rods of approximately 5-mm diameter for XPS measurements. X-ray powder diffraction analysis indicated that the glasses formed were completely amorphous and no alumina was detected within the resolution limits in either the XPS spectra or the compositional analyzes. The actual compositions of the glasses were subsequently determined by inductively coupled plasma spectroscopy (ICP) and are listed in Table 1.

2.2. X-ray photoelectron spectroscopy (XPS) measurements

Core level photoelectron spectra were collected on a VG Scientific ESCALAB MKII spectrometer equipped with dual aluminum–magnesium anodes using Al Kα radiation ($h\nu = 1486.6$ eV) from an anode operated at 130 W. For self-consistency, the C 1s line at 284.6 eV was used as a reference for all charge shift corrections as this peak arises from hydrocarbon contamination and its binding energy is generally accepted as remaining constant, irrespective of the chemical state of the sample. For XPS measurements, a glass rod from each composition was cleaved in the preparation chamber at a base pressure of 2×10^{-9} mbar before being transferred to the analysis chamber where the pressure was maintained at $<2 \times 10^{-10}$ mbar. A non-linear, least-squares algorithm was employed to determine the best fit to each of the O 1s, V 2p, and P 2p spectra with two-to-four Gaussian–Lorentzian curves in order to represent various oxygen bonding sites (e.g., P–O–P, P–O–V, V–

Table 1
Peak positions, FWHM, areas, and relative abundance from the curve fitting of the O 1s and P 2p core levels for various vanadium phosphate $(V_2O_5)_x(P_2O_5)_{1-x}$ glasses. Actual compositions (5%) were determined from ICP measurements.

x (nominal)	x (actual)	O 1s (I) FWHM area abundance	O 1s (II) FWHM area abundance	O 1s (III) FWHM area abundance	O 1s (IV) FWHM area abundance	P 2p FWHM (single-peak)	P $2p_{3/2}$ FWHM area abundance	P $2p_{1/2}$ FWHM area abundance	Ratio of P 2p areas
0.30	0.36	533.10 2.27 7577 0.285	531.28 2.10 17359 0.652	529.56 1.17 1709 0.064	528.43 2.05 4929 –	133.81 2.65	133.55 1.95 4172 0.685	134.45 1.95 1923 0.315	2.17
0.40	0.39	533.08 2.27 8362 0.304	531.26 2.06 18540 0.675	529.50 1.23 574 0.021	–	133.73 2.80	133.40 2.10 4564 0.677	134.45 2.10 2176 0.323	2.10
0.50	0.46	532.99 2.29 11947 0.286	531.42 1.94 29876 0.714	–	–	133.65 2.94	133.35 2.00 4422 0.679	134.40 2.00 2095 0.321	2.11
0.60	0.54	533.18 2.23 7893 0.165	531.47 2.09 39811 0.835	–	–	133.97 2.69	133.65 2.05 3406 0.672	134.70 2.05 1665 0.328	2.05

The uncertainty in the peak positions is ±0.1 eV, FWHM ±0.2 eV, and areas ±10%.

O–V, P=O, and V=O), different vanadium oxidation states (V^{5+}, V^{4+}, and V^{3+}), and a possible spin–orbit splitting in the phosphate core level. The fraction (relative abundance) of various oxygen bonding sites, V^{5+}, V^{4+}, and V^{3+} ions, and P $2p_{1/2}$ and P $2p_{3/2}$ levels were determined from the respective area ratios obtained from these fits. Based on the reproducibility of similar quantitative spectral decompositions of spectra taken from other surfaces on the same glass samples, uncertainties of ±10% for the various oxygen bonding sites, the V^{n+} concentration and P 2p levels were estimated from these area ratios. A period of approximately two hours was required to collect the data set for each sample.

2.3. Magnetic measurements

The temperature-dependent DC magnetic susceptibility (M/H where M is the magnetization and H the magnetic field) was measured using a SQUID magnetometer (Quantum Design model MPMS-5S) in a magnetic field of 5000 Oe over a temperature range of 5–300 K at temperature intervals of 2.5 K. The susceptibility of the sample holder is negligible for all samples and the overall accuracy of the magnetic measurements is estimated to be approximately 3% due to the uncertainty of the magnetometer calibration.

3. Results

High-resolution XPS spectra for the O 1s core level of these V_2O_5–P_2O_5 glasses are shown in Fig. 1. While the O 1s peak positions for all samples appear to be essentially the same, all spectra show an asymmetry on the higher binding energy side of the peaks with this asymmetry being greatest for the nominal $x = 0.30$ and 0.40 samples. In addition another feature is evident around 528.5 eV in the spectrum for the $x = 0.30$ sample. The appearance of an asymmetry in the O 1s spectra is not unexpected as it is well-known that the O 1s peak in glasses can arise from different oxygen binding sites. Typically a higher energy contribution arises from the presence of bridging oxygen (BO) atoms and a second lower energy peak results from the non-bridging oxygen (NBO) atoms [25–29]. Thus the O 1s spectra for the $x \geqslant 0.40$ samples were initially fitted to two Gaussian peaks as shown in Fig. 2(a) and (b) on top of a downward-sloping linear background. However upon closer inspection of the overall two-peak fit with linear background to the $x = 0.40$ spectra (not shown), the fit below 530 eV was less satisfactory in comparison to the others. Moreover the FWHM (full-width at half-maximum) value resulting from the two-peak fitting routine for the lower peak of the $x = 0.40$ spectrum is much larger which is indicative of the need to include a third peak in the fitting of the spectrum. Consequently a three-peak fit was undertaken as shown in Fig. 2(c). For the $x = 0.30$ spectrum, the same downward-sloping linear background as employed in the fits for the other compositions was used as well as a broad Gaussian to account for the increasing signal for energies below 527 eV which was observed in all four samples. The resulting main peak after this background subtraction was similarly deconvoluted into three peaks as well as including a fourth Gaussian peak to account for the feature at 528.5 eV as shown in Fig. 2(d). The resulting peak positions, FWHM, areas under the peaks, and relative abundance of the different oxygen sites labeled as I, II, III, and IV are displayed in Table 1. As seen in Table 1 from these fits, the peak positions for O 1s (I) and O 1s (II) of 533.1 and 531.3 eV, respectively, show little dependence on the V_2O_5 content with the relative abundances under the O 1s (I) and O 1s(II) peaks remaining relatively constant for glasses with $x \leqslant 0.50$.

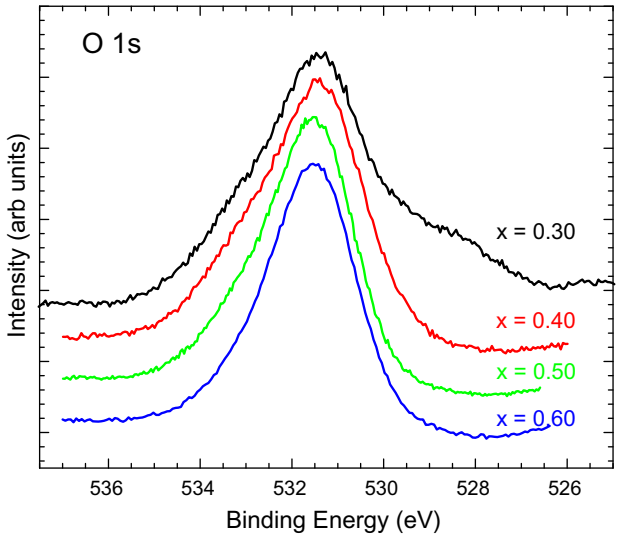

Fig. 1. Core level O 1s spectra for the $(V_2O_5)_x(P_2O_5)_{1-x}$ glasses.

Similar to the characteristics of the O 1s peaks, the position of the P 2p core level peak as shown in Fig. 3 appears to have little concentration dependence although the peak for the nominal $x = 0.60$ glass composition appears to be slightly shifted to higher energy (≈0.2–0.3 eV) as compared to those of the three other concentrations. Furthermore, since the P 2p peaks are more symmetric than those of the O 1s spectra, each spectrum was initially fit to a single peak which resulted in the peak position and FWHM values displayed in Table 1. Although the peak positions are in good agreement with the analyzes of the P 2p spectra from our previous XPS investigations on a series of different phosphate glasses [30–31], the peaks are broader as the FWHM values are 30–40% larger. Moreover, some asymmetry is noticeable in the spectra for the $x = 0.30$ and 0.40 glass samples. As a result, each P 2p spectrum was deconvoluted into two Gaussian peaks labeled P $2p_{3/2}$ and P $2p_{1/2}$ as seen by the fitting of the spectral data in Fig. 4. The peak positions for P $2p_{3/2}$ and P $2p_{1/2}$ of 133.5 and 134.5 eV, respectively, exhibit little dependence on V_2O_5 content with the ratios of the areas (relative abundance) under their peaks equaling about 2.1 and being relatively independent of V_2O_5 concentration as seen in Table 1.

Fig. 5 shows the core level spectra of V 2p for the V_2O_5–P_2O_5 glass samples and the peak positions are in relatively good agreement with those reported on other vanadate glasses [29,32]. Although upon more careful inspection of the V $2p_{3/2}$ spectra, an asymmetry is clearly observable on the lower binding energy side of the core level, which is indicative of vanadium ions existing in more than one oxidation state. Hence, the main peak around 516 eV in each V $2p_{3/2}$ spectrum was initially fitted to two Gaussian–Lorentzian peaks with the lower binding energy peak (labeled V $2p_{3/2}(1)$) corresponding to V^{4+} and the higher binding energy peak (labeled V $2p_{3/2}(2)$) to V^{5+} while the satellite peak around 520.5 eV was fit to single Gaussian–Lorentzian peak as shown in Fig. 6(a). Since this satellite peak has been previously observed in the spectrum of pure V_2O_5 [29], it will also be associated with V^{5+}. Table 2 displays the result of these two-peak + satellite fits including the peak positions and relative abundance of V^{4+}/V_{total}, which varies from about 67% for the $x = 0.30 - 0.50$ samples to 55% for the glass sample with $x = 0.60$. Since an earlier report [24] suggested that even lower oxidation states for vanadium might be present for smaller V_2O_5 containing phosphate glasses, the main peaks around 516 eV in all V $2p_{3/2}$ spectra were also fitted to three Gaussian–Lorentzian peaks representing V^{3+}, V^{4+}, and V^{5+} as shown in Fig. 6(b). The corresponding parameters from fitting three peaks are likewise displayed in Table 2 along with the

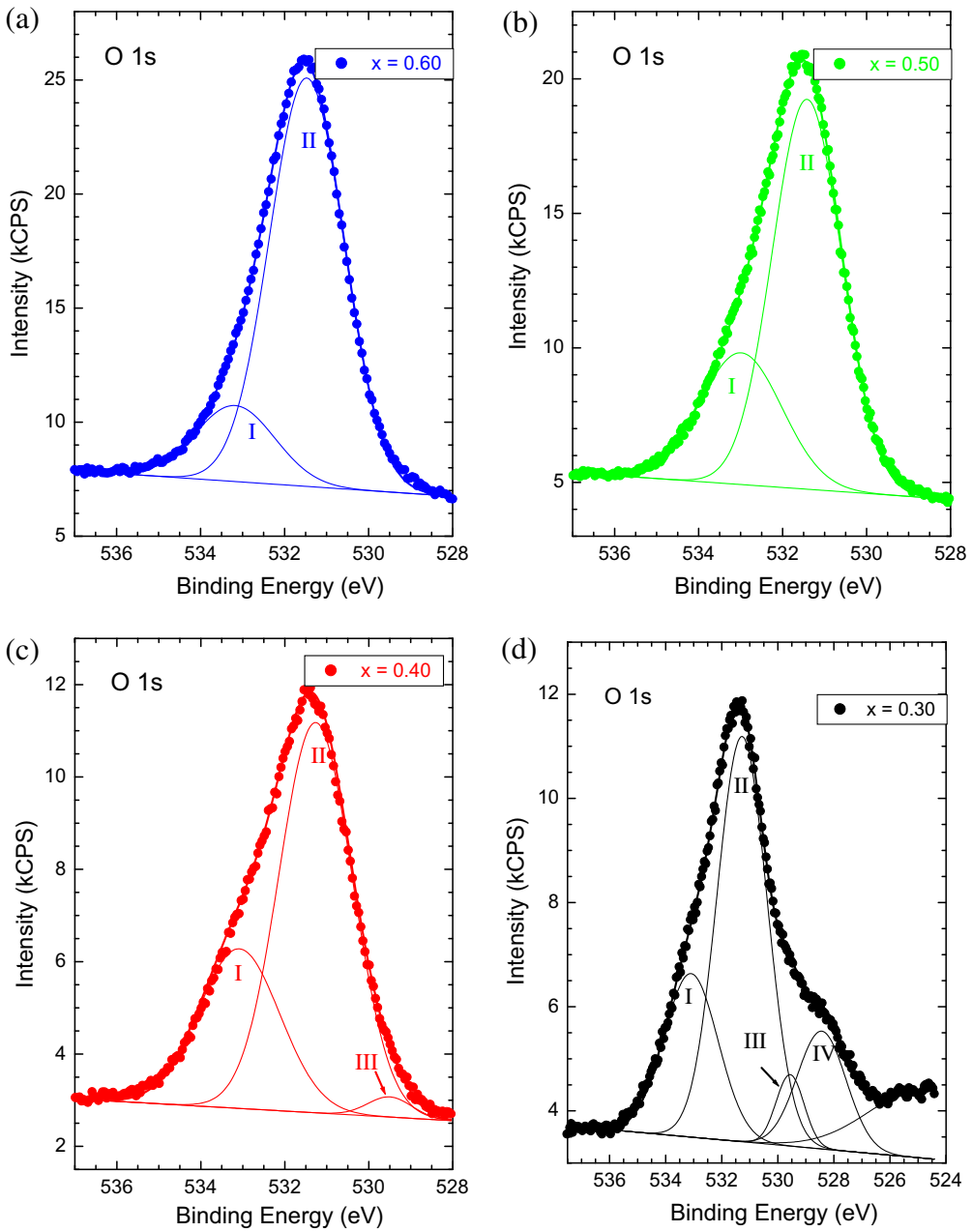

Fig. 2. High-resolution O 1 s spectra for the $(V_2O_5)_x(P_2O_5)_{1-x}$ glass samples and the resulting peaks from the least-squares Gaussian fitting routine. The smooth solid line is the resultant sum of the peaks plus the background.

corresponding average valence n of the vanadium ions based on the relative areas under each of the three peaks.

The temperature T dependence of the magnetic susceptibility data for all glass samples appear to follow a Curie–Weiss behavior, $M/H = C/(T-\theta)$, with a temperature-independent background. After determining the background contribution from a high-temperature extrapolation of M/H-vs-$1/T$ plots, the resulting M_{corr}/H ($=M/H-(M/H)_{background}$) data were found to follow a Curie–Weiss behavior, $M_{corr}/H = C/(T-\theta)$, with the Curie constant C and the paramagnetic Curie temperature θ determined from the least-squares fits of the H/M_{corr}-vs-T data as shown in Fig. 7. Table 3 displays these parameters ($(M/H)_{background}$, C, and θ) for each of the glass samples. From the Curie constant C, the relative fraction of V^{4+} ($\mu_{eff} = 1.8\ \mu_B$) was determined assuming that only V^{4+} and V^{5+} ($\mu_{eff} = 0\ \mu_B$) ions were present in these glasses.

4. Discussion

As described in the preceding section, the peak positions and FWHM of the P 2p core levels appear to be fairly independent of the vanadium content from the single-peak fits to the P 2p spectra. However, the observed broadness and asymmetry in the peaks which resulted in the deconvolution of the P 2p spectra into two peaks could arise from the spin–orbit splitting of the P 2p core level resulting in distinguishable P $2p_{3/2}$ and P $2p_{1/2}$ core levels with the lower binding energy peak corresponding to P $2p_{3/2}$. Since the predicted P $2p_{3/2}$/P $2p_{1/2}$ ratio of 2.0 [33] is within the uncertainty of the measured ratios of the relative areas of 2.1 ± 0.1, it is reasonable to conclude that the asymmetry in the P 2p spectra indeed arises from this spin–orbit splitting of the P 2p core level.

Upon comparing the relative ratios of V^{4+}/V_{total} in Tables 2 and 3, the fitting of the V $2p_{3/2}$ spectra to two Gaussian–Lorentzian peaks

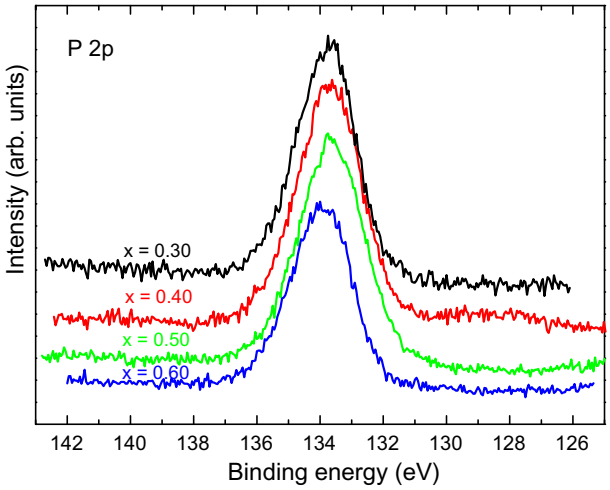

Fig. 3. Core level P 2p spectra for the $(V_2O_5)_x(P_2O_5)_{1-x}$ glasses.

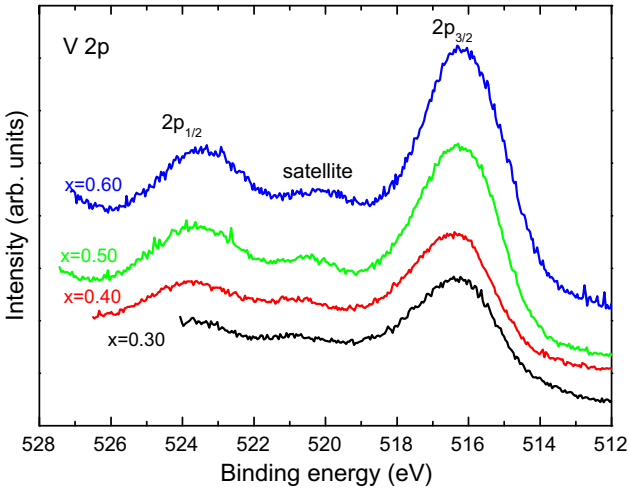

Fig. 5. Core level V 2p spectra for the $(V_2O_5)_x(P_2O_5)_{1-x}$ glasses.

with the lower binding energy peak corresponding to V^{4+} and the higher binding energy peaks to V^{5+} leads to some quantitative inconsistency with the magnetic analysis. The corresponding relative abundance of V^{4+}/V_{total} as determined from the areas under the two peaks showed a significant difference between the $x = 0.30 - 0.50$ samples and the $x = 0.60$ sample, an average of 67% compared to 55%, respectively. Although a similar large decrease in the ratios of V^{4+}/V_{total} between the $x \leqslant 0.50$ and 0.60 glass samples was found from the magnetic susceptibility determinations, the quantitative agreement is poorer for the $x \leqslant 0.50$ compositions. In fact, the determination from the Curie constant for the $x = 0.30$ sample would require 119% V^{4+} which is not physically possible. Instead, the presence of V^{3+} ions, which have larger magnetic moment ($\mu_{eff} = 2.8\ \mu_B$), in addition to V^{4+} and V^{5+} ions could provide a plausible explanation for the larger than expected Curie constant. Consequently the fitting of the V 2p core level spectra to three Gaussian–Lorentzian peaks corresponding to V^{3+}, V^{4+}, and V^{5+} as shown in Fig. 6(b) would seem to be justifiable. The relative abundances of V^{3+}/V_{total}, V^{4+}/V_{total}, and V^{5+}/V_{total} from this fitting procedure are also listed in Table 2 along with the average valence n for the vanadium ions based on the relative weighting of these three abundances. Unfortunately a completely independent analysis of the magnetic results with three different V ions being present cannot be undertaken since only one independent variable, i.e., the concentration of one oxidation state of the V ions, can be determined from the measured values of the Curie constant. Nevertheless, a comparison between the XPS and magnetic measurements was attempted by: (i) calculating the Curie constant $C_{calculated}$ from the relative percent of V^{3+}/V_{total}, V^{4+}/V_{total} V^{5+}/V_{total} from the XPS analysis listed in Table 2; and (ii) using the V^{4+} relative percentage as determined by the XPS three-peak fitting from Table 2 and then determining the V^{5+} and V^{3+} percent present from the measured Curie constant. In either approach, the agreement is within 10%, as shown in Table 3 which is reasonable considering the 10% uncertainty in determining the percents from the areas under the peaks in the XPS spectra. Thus it is highly probable that these

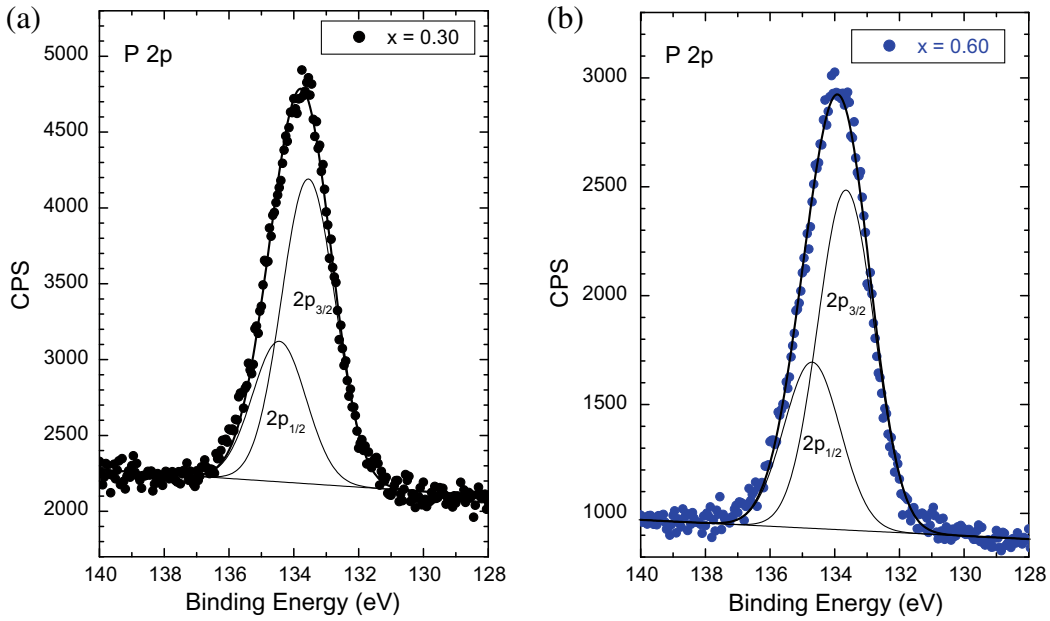

Fig. 4. High-resolution P 2p spectra for the (a) $x = 0.30$ and (b) $x = 0.60$ V_2O_5 phosphate glass samples and the resulting P $2p_{1/2}$ and P $2p_{3/2}$ peaks from the least-squares fitting of two Gaussian peaks. The smooth solid line is the resultant sum of the two-peaks plus the background.

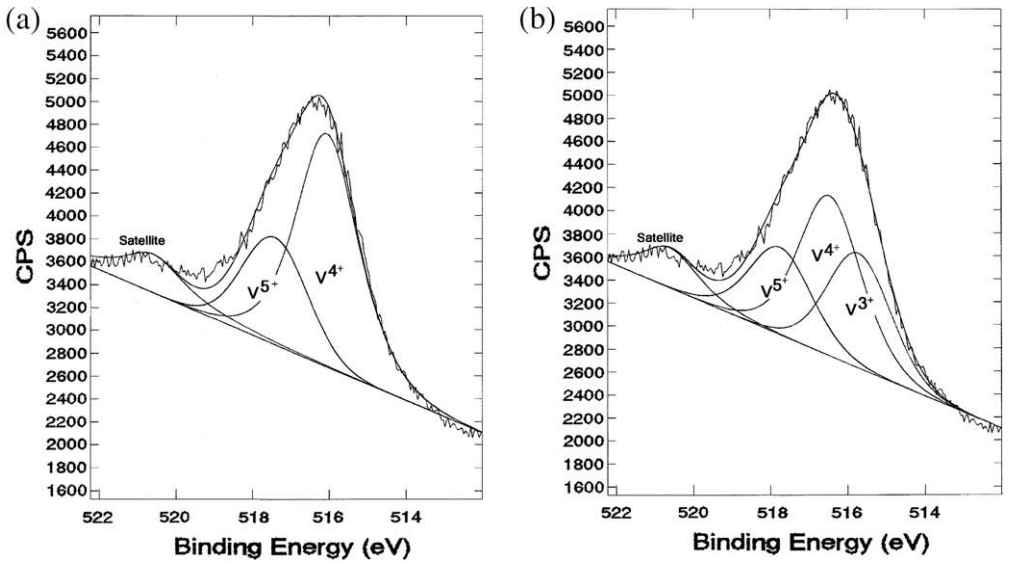

Fig. 6. High-resolution V 2p spectra for the $x = 0.30$ V_2O_5 phosphate glass sample (a) with the resulting V^{5+} and V^{4+} peaks from the least-squares fitting of two Gaussian–Lorentzian peaks and (b) with the resulting V^{5+}, V^{4+}, and V^{3+} peaks from the least-squares fitting of three Gaussian–Lorentzian peaks. The smooth solid line in both figures is the resultant sum of the peaks plus the background.

Table 2
Peak positions, FWHM, and relative abundances (relative areas) of the various V ions from the curve fitting of the V 2p core levels + satellite peak for the V_2O_5 phosphate glasses.

x	Two-peak + satellite fitting				Three-peak + satellite fitting							
	$V2p_{3/2}$(sat) FWHM area	$V2p_{3/2}(1)$ FWHM area	$V2p_{3/2}(2)$ FWHM area	Area(1)/ total area = V^{4+}/V_{total}	$V2p_{3/2}$(sat) FWHM area	$V2p_{3/2}(1)$ FWHM area	$V2p_{3/2}(2)$ FWHM area	$V2p_{3/2}(3)$ FWHM area	Area(1)/ total area = V^{3+}/V_{total}	Area(2)/ total area = V^{4+}/V_{total}	[Area(3) + area(sat)]/ total area = V^{5+}/V_{total}	Average valence, n
0.30	520.60 2.00 326	516.06 2.00 4461	517.42 2.00 1989	0.658	520.60 1.80 377	515.71 2.00 2071	516.46 2.00 2965	517.74 2.00 1591	0.296	0.423	0.281	3.98
0.40	520.54 1.90 17	516.24 2.00 3955	517.61 2.00 1730	0.694	520.54 1.90 16	515.71 2.00 1060	516.46 2.00 3270	517.74 2.00 1424	0.184	0.567	0.250	4.07
0.50	520.52 1.90 281	516.24 2.00 8624	517.61 2.00 3934	0.672	520.54 1.90 90	515.71 2.00 1181	516.46 2.00 8809	517.74 2.00 1932	0.098	0.733	0.168	4.07
0.60	520.30 1.94 305	516.19 2.00 4277	517.29 2.00 3230	0.547	520.30 1.94 305	–	516.19 2.00 4277	517.29 2.00 3230	–	0.547	0.453	4.45

The uncertainty in the peak positions is ±0.1 eV, FWHM ±0.2 eV, and the relative areas ±10%.

glasses with the lower V_2O_5 ($x \leqslant 0.50$) content contain V^{3+} in addition to V^{4+} and V^{5+} ions. Moreover, with less than 25% of the vanadium ions existing in the V^{5+} valence state for these lower V_2O_5 ($x \leqslant 0.50$) containing glasses, local glass structures with VO_6 octahedras may be more prevalent than structures with the VO_5 trigonal bipyramids.

While the cation spectra provide some insight into the structure of these oxide glasses, the O 1s spectra are typically more informative as the binding energy of the O 1s electrons provides a measure of the extent to which electrons are localized on the oxygen or in the internuclear region, which is a direct consequence of the nature of the bonding between the oxygen and different cations. Correspondingly, the O 1s peaks for these V_2O_5–P_2O_5 glasses may arise from oxygen atoms existing in some or all of the following structural bonds: P–O–P, P–O–V, V–O–V, V=O, and P=O. Furthermore, the O1s peaks associated with these various structural bonds may be broaden by the vanadium ions existing in different valence states. Oxygen atoms that are more covalently bonded to glass former atoms on both sides are typically called bridging oxygen (e.g., P–O–P, V–O–V), while oxygen atoms that are more ionically bonded, at least on one side, or double-bonded to a glass former atom are referred to as non-bridging oxygen atoms and have lower binding energies (e.g., P–O–Na, V–O–Sr, P=O, V=O). Since the glass former in the vanadate phosphate glass system may actually change from phosphate to vanadate depending upon the vanadium content, the relative ionic nature of the various bonds can be examined in order to assign the various O 1s peaks to the appropriate oxygen bonding structures. Based on the Pauling electronegativity of P (2.19) being greater than that for V (1.63), the P–O–P bond would be the most covalent, followed by the P–O–V bond and then the V–O–V bond with the V=O bond being the most ionic. Correspondingly, the binding energy for each structural bond should be lower, which is consistent with the results from previous XPS studies. For example, binding energies of 534.2 eV and 532.4 eV have been determined for P–O–P and P–O–TM bonds, respectively, in Zn and Fe-doped phosphate glasses [9,26] while the respective values of 533.3 eV and 531.7 eV were found in Mo-doped phosphate glasses [34,35]. Moreover the binding energies for V–O–V and V–O–TM/V=O structures have been reported to be closer to 531.6–530.9 and 530.3–529.9 eV, respectively [28,30,32].

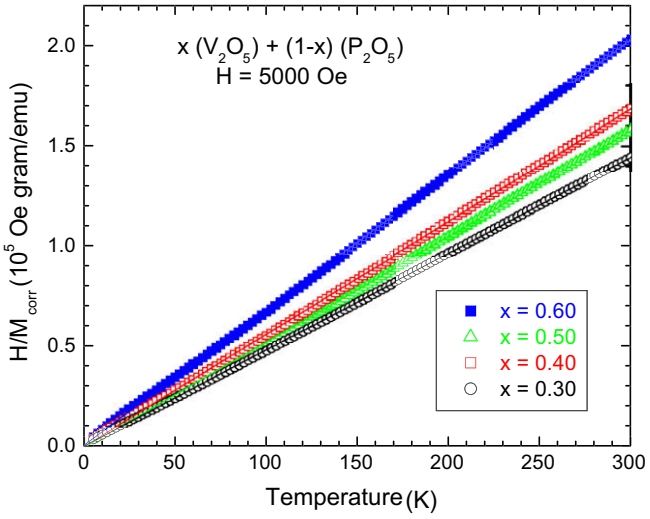

Fig. 7. The inverse of the "corrected" magnetic susceptibility M_{corr}/H ($= M/H - M_{background}/H$) as a function of the temperature T for the $(V_2O_5)_x(P_2O_5)_{1-x}$ glasses.

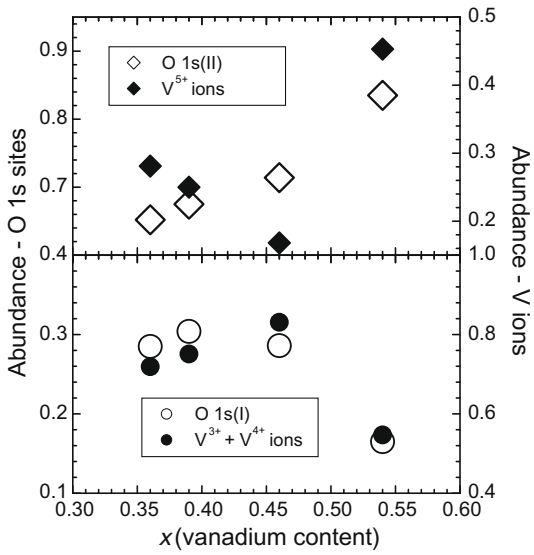

Fig. 8. The abundance per $(V_2O_n)_x{\cdot}(P_2O_5)_{1-x}$ molecule of the O 1s (I) and O 1s (II) atoms and the various V ions as a function of the actual vanadium content, x.

Therefore, it is reasonable to conclude that the O 1s (I) peak at 533.1 eV should be associated with P–O–P structural bonds and that the O 1s (II) peak at 531.3 eV should be identified with both P–O–V and V–O–V bonds. The smaller O 1s (III) peak at 529.6 eV would correspondingly be identified as a V=O site or possibly a V^{4+}–O–V^{3+} bond which would be even more ionic than a V^{n+}–O–V^{n+} structure. Lastly since the O 1s (IV) peak occurs at a binding energy is well below any previously identified V–O–TM bonds, this peak is more likely an experimental artifact resulting from a contamination effect that could have arisen during the cleavage process.

Based on the assignment of these various O 1s peaks, the nature of the glass structure can now be explored more quantitatively by comparing the relative area under each peak to the predicted number (relative abundance) of P–O–P, P–O–V, and V–O–V bonds arising from different vanadium phosphate glass structures. As noted previously, the simple structural depolymerization model of a binary phosphate glass [8] should result in about 10% P–O–P bonds from the Q^1 pyrophosphate structures for the $x = 0.30$ sample assuming all vanadium are in the V^{5+} valence state. However, the larger relative abundances of P–O–P bonds (areas under the O 1s(I) peak) for all samples of 30%-to-17% and the relatively large fraction of V ions being in the non-5+ valence state indicate that a more complex structural model is clearly needed. As a first step, the abundances of the O 1s atoms are compared to the abundances of the V ions in various valence states. Fig. 8 displays these abundances per $(V_2O_n)_x{\cdot}(P_2O_5)_{1-x}$ molecule as a function of the actual vanadium content x where the total number of oxygen atoms is given $[5(1-x) + nx]$ and n is the average valence of the vanadium ions. One immediately notes the qualitative correlation of the abundances of the O 1s (II) and O 1s (I) atoms with the respective abundances of the V^{5+} ions and the $V^{4+} + V^{3+}$ ions for these four glass compositions as the abundance of the O 1s (II) atoms tends to increase dramatically when the abundance of V^{5+} ions increases and the abundance of the $V^{4+} + V^{3+}$ ions decreases for the $x = 0.60$ sample. Likewise, the abundance of O 1s (I) atoms shows a decrease when the abundance of V^{5+} ions increases and the abundance of the $V^{4+} + V^{3+}$ ions decreases. Since the O 1s (II) atoms have been tentatively indentified as representing P–O–V and V–O–P bonds while the O 1s (I) atoms as P–O–P bonds, these correlations of the abundances suggest that the local glass structure of this glass system is composed of at least two different structures. (i) The PO_4 tetrahedras associated with the local glass structure containing the V^{5+} ions are probably isolated units with no oxygen in P–O–P bonding sites. (ii) On the other hand, the PO_4 tetrahedras associated with the $V^{4+} + V^{3+}$ local structures probably are more likely to be a mixture of meta-, pyro-, and orthophosphate structures, i.e., $(PO_3)^{1-}$, $(P_2O_7)^{4-}$, and $(PO_4)^{3-}$, with two, one, and zero P–O–P bonding sites per phosphate unit, respectively. While this picture accounts for the qualitative tendencies, a more quantitative comparison would require a more refined model of the local glass structure.

The next step would be to build a model based on the assumption that the glass consists of a mixture of structural groupings that occur in the crystalline phases. These would include V_2O_5 and $VOPO_4$ for the V ions in the 5+ valence state, $(VO)_2P_2O_7$ and $VO(PO_3)_2$ for the V^{4+} ions, and $V(PO_3)_3$ for the V^{3+} ions [36–40]. For compositions of these mixed-valence vanadium phosphate glasses written in the form:

$$xV_2O_5\ yV_2O_4\ zV_2O_3\ (1-x-y-z)P_2O_5,$$

Table 3
Magnetic susceptibility results for the $(V_2O_5)_x(P_2O_5)_{1-x}$ glasses and comparison of concentrations of various V^{n+} ions to total vanadium ions from magnetic and XPS measurements.

x (nominal)	x (actual)	Magnetic measurements				XPS measurements			
		$(M/H)_{background}$ $\left(\frac{10^{-7}\ emu}{g\ Oe}\right)$	C $\left(\frac{10^{-3}\ emu\ K}{g\ Oe}\right)$	θ (K)	V^{4+}/V_{total}	$C_{calculated}$ $\left(\frac{10^{-3}\ emu\ K}{g\ Oe}\right)$	V^{4+}/V_{total} from XPS	V^{5+}/V_{total} from measured C	V^{3+}/V_{total} from measured C
0.30	0.36	−3.77	2.15	−1.91	1.19	2.17	0.423	0.301	0.276
0.40	0.39	−1.69	1.80	−1.68	0.94	2.04	0.567	0.298	0.135
0.50	0.46	−4.30	2.00	−1.75	0.89	2.23	0.733	0.224	0.043
0.60	0.54	4.40	1.41	−1.53	0.55	1.41	0.547	0.441	0.012

where x, y, and z are the mole fractions of V^{5+}, V^{4+}, and V^{3+} ions, respectively, the corresponding mole fractions of the structural groupings would be given by:

$$\left[\frac{2x}{1-y-2z}\right]VOPO_4\left[\frac{4z+3y+2x-1}{1-y-2z}\right](VO)_2P_2O_7\left[\frac{2-4x-4y-8z}{1-y-2z}\right] \times VO(PO_3)_2\left[\frac{2z}{1-y-2z}\right]V(PO_3)_3$$

for the glasses with the lowest two concentrations of vanadium, and

$$\left[\frac{4z+2y+2x-1}{1-y-2z}\right]V_2O_5\left[\frac{2-2x-4y-8z}{1-y-2z}\right]VOPO_4\left[\frac{y}{1-y-2z}\right] \times (VO)_2P_2O_7\left[\frac{2z}{1-y-2z}\right]V(PO_3)_3$$

for the glasses with the highest two concentrations of vanadium. Using the relative abundances of V^{5+}, V^{4+}, and V^{3+} as determined by the areas under the V 2p peaks in Table 1, the fraction of oxygen in the P–O–P sites to the total number of oxygen sites are correspondingly found to vary from 0.21 for the nominal $x = 0.30$ sample to 0.06 for the nominal $x = 0.60$ sample, significantly lower than the measured values of 0.30 for the $x \leqslant 0.50$ samples and 0.17 for the x = 0.60 sample as determined by the areas under the O 1s (I) peaks in Table 1. These differences are not too surprising given the multiple valence states of vanadium existing in these samples and the simplistic nature of this model. Moreover, the analysis of the O 1s peaks may actually require a deconvolution into four separate peaks instead of three peaks in order to account for the difference in the binding energies for the P–O–V and V–O–V bonding sites. The highest energy peak would still be associated with the P–O–P bonds, but a second peak for the P–O–V bonds separate from a third peak for the V–O–V bonds would be required in addition to the lowest energy peak associated with the V=O bonds. This four-peak fit would basically result in the present O 1s (I) and O 1s (II) peaks becoming three peaks and the area under the O 1s (I) peak becoming smaller, in better quantitative agreement to the preceding model. Unfortunately, such an analysis has an overabundance of fitting parameters (peak position, FHWM, area for each peak) that a non-unique fit could not be found, making further quantitative comparisons less meaningful. Nevertheless, the qualitative agreement of the abundance of orthophosphate $(PO_4)^{3-}$ units with non-bonding O sites increasing when the abundance of V^{5+} ions increased and the abundance of $V^{4+} + V^{3+}$ ions decreased for the nominal $x = 0.60$ sample is consistent with the proposed mixture of structural groupings that occur in the crystalline phases.

5. Conclusions

XPS has been used to investigate the local glass structure on a series of V_2O_5–P_2O_5 glasses. For increasing V_2O_5 concentrations, the O 1s spectra owing to an asymmetry in the peak structure indicate a decreasing abundance of the bridging oxygen relative to the non-bridging oxygen as evidenced by the reduction of the area under the highest binding energy peak. To account for this feature, the bridging oxygen are associated with the P–O–P bonds since these bonds would be more covalent and have a higher binding energy while those in the P–O–V and V–O–V bonds are more probably of an ionic nature and have lower binding energies. Likewise the P 2p spectra display an asymmetry which can be described in terms of a spin–orbit splitting of the P 2p core level. Analysis of the V 2p spectra as well as the magnetic results indicates the presence of multiple valence states for vanadium. Qualitative comparisons of the abundance of the bridging oxygen sites with the abundances of the various phosphate structural groups and valence states of the vanadium ions suggest a glass structural model consisting of a mixture of phosphate structures for these samples, including V_2O_5, $VOPO_4$, $(VO)_2P_2O_7$, $VO(PO_3)$, and $V(PO_3)_3$.

Acknowledgments

The support of the KFUPM Physics Department and Research Committee (Grant PH/Glasses/346) is greatly acknowledged. In addition the authors wish to acknowledge the assistance of Dr. G.M. Tsoi with the magnetic susceptibility measurements and discussions of the results with Dr. V. Dimitrov.

References

[1] A. Ghosh, J. Appl. Phys. 64 (1988) 2652.
[2] A. Ghosh, Phys. Rev. B 42 (1990) 5665.
[3] J. Livage, J.P. Jollivet, E. Tronc, J. Non-Cryst. Solids 121 (1990) 35.
[4] N. Ichinose, Y. Nakai, J. Non-Cryst. Solids 203 (1996) 353.
[5] N.F. Mott, J. Non-Cryst. Solids 1 (1968) 1.
[6] I.G. Austin, N.F. Mott, Adv. Phys. 18 (1969) 41.
[7] J.H. Campbell, T.J. Suratwala, J. Non-Cryst. Solids 263&264 (2000) 318.
[8] R.K. Brow, J. Non-Cryst. Solids 263&264 (2000) 1.
[9] R.K. Brow, J. Non-Cryst. Solids 194 (1996) 267.
[10] R.K. Brow, D.R. Tallant, S.T. Myers, C.C. Phifer, J. Non-Cryst. Solids 191 (1995) 45.
[11] R.K. Brow, C.A. Click, T.M. Alam, J. Non-Cryst. Solids 274 (2000) 9.
[12] E. Lippma, M. Magi, A. Samoson, G. Englehardt, A.R. Grimmer, J. Am. Ceram. Soc. 102 (1980) 4889.
[13] S. Hayakawa, T. Yoko, S. Sakka, J. Ceram. Soc. Jpn. 102 (1994) 522.
[14] S. Hayakawa, T. Yoko, S. Sakka, J. Ceram. Soc. Jpn. 102 (1994) 530.
[15] S. Hayakawa, T. Yoko, S. Sakka, J. Non-Cryst. Solids 183 (1995) 73.
[16] A.C. Wright, Phil. Mag. B 50 (1984) 23.
[17] A.C. Wright, C.A. Yarker, P.A.V. Johnson, R.N. Sinclair, J. Non-Cryst. Solids 76 (1985) 333.
[18] S. Sen, A. Ghosh, J. Non-Cryst. Solids 258 (1999) 29.
[19] S. Sen, A. Ghosh, J. Mater. Res. 15 (2000) 995.
[20] Y. Dimitriev, V. Dimitrov, M. Arnaudov, D. Topalov, J. Non-Cryst. Solids 57 (1983) 147.
[21] M. Nabavi, C. Sanchez, J. Livage, Phil. Mag. B 63 (1991) 941.
[22] J. Mendialdua, R. Casanova, Y. Barbaux, J. Electron Spectrosc. Relat. Phenom. 71 (1995) 249.
[23] F.R. Landsberger, P.J. Bray, J. Chem. Phys. 53 (1970) 2757.
[24] H. Harper, P.W. McMillan, Phys. Chem. Glasses 15 (1974) 148.
[25] R.K. Brow, in: R.E. Loehman (Ed.), Characterization of Ceramics, Butterworth-Heinemann, London, 1993.
[26] R.K. Brow, C.M. Arens, X. Yu, E. Day, Phys. Chem. Glasses 35 (1994) 132.
[27] B.M.J. Smets, D.M. Krol, Phys. Chem. Glasses 25 (1984) 113.
[28] G.D. Khattak, M.A. Salim, L.E. Wenger, A.H. Gilani, J. Non-Cryst. Solids 262 (2000) 66.
[29] A. Mekki, G.D. Khattak, L.E. Wenger, J. Non-Cryst. Solids 330 (2003) 156.
[30] G.D. Khattak, E.E. Khawaja, L.E. Wenger, D.J. Thompson, M.A. Salim, A.B. Hallak, M.A. Daous, J. Non-Cryst. Solids 194 (1996) 1.
[31] M.A. Salim, G.D. Khattak, P.S. Fodor, L.E. Wenger, J. Non-Cryst. Solids 289 (2001) 185.
[32] G.D. Khattak, N. Tabet, L.E. Wenger, Phys. Rev. B 72 (2005) 104203.
[33] J.F. Moulder, W.F. Stickle, P.E. Sobol, K.D. Bomben, Handbook of X-ray Photoelectron Spectroscopy, Perkin-Elmer, Eden Prairie, MN, USA, 1992. p. 22.
[34] B.V.R. Chowdari, K.L. Tan, W.T. Chia, R. Gopalakrishan, J. Non-Cryst. Solids 119 (1990) 95.
[35] G.D. Khattak, M.A. Salim, A.S. Al-Harthi, D.J. Thompson, L.E. Wenger, J. Non-Cryst. Solids 212 (1997) 180.
[36] B. Jordan, C. Calvo, Can. J. Chem. 51 (1973) 2621.
[37] S. Geupel, K. Pilz, S. van Smaalen, F. Büellesfeld, A. Prokofiev, W. Assmus, Acta Cystallogr. C58 (2002) 9.
[38] E.V. Murashova, N.N. Chudinova, Kristallografiya 39 (1994) 145.
[39] K.-H. Lii, Y.B. Chen, C.C. Su, S.-L. Wang, J. Solid State Chem. 82 (1989) 156.
[40] E. Benser, R. Glaum, T. Dross, H. Hibst, Chem. Mater. 19 (2007) 4341.